MEMS 2017

# Conference Proceedings

## The 3rd Conference on MicroFluidic Handling Systems

4-6 October 2017

Enschede
The Netherlands


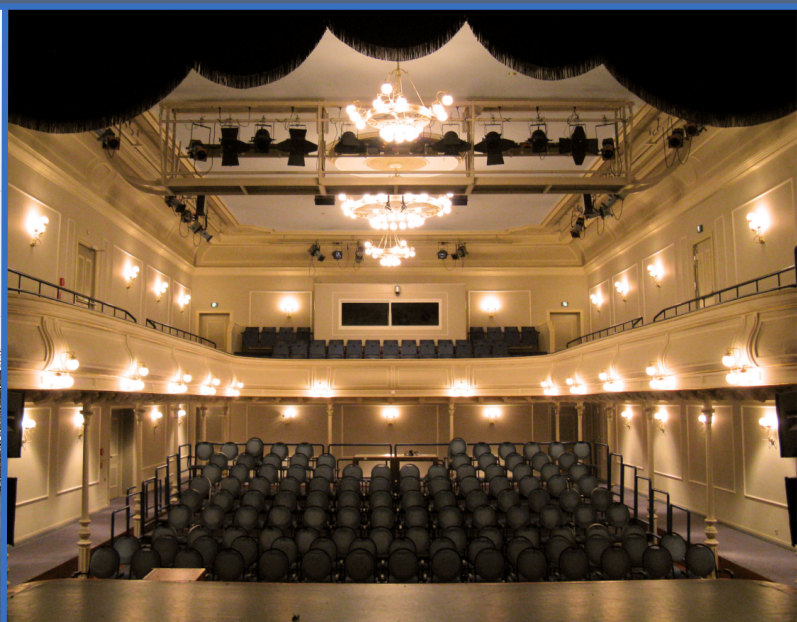

**Conference:** The 3rd Conference on MicroFluidic Handling Systems (MFHS 2017).
**Dates:** 4-6 October 2017.
**Chairs:** Joost Lötters and Gerald Urban.
**Technical program committee:** Ellis Meng, Shuichi Shoji, Jens Ducrée, Wouter van der Wijngaart, Bernhard Jakoby, Nico de Rooij, Peter Koltay, Andreas Ernst, Andreas Manz, Jankees Hogendoorn, Paddy French, Remco Wiegerink, Niels Tas.
**Sponsors:** University of Twente, MESA+, Bronkhorst High-Tech, Krohne, Innovative Sensor Technology IST AG, Fluigent, BioFluidiX, MDPI Micromachines, TNO, LioniX, Kloé, Micronit Microtechnologies, Truedyne, Axetris and Hahn-Schickard.
**Location:** De Kleine Willem, Langestraat 45, 7511 HB Enschede, The Netherlands.
**Organization:** Remco Wiegerink, Susan Janse, Dennis Alveringh. Jarno Groenesteijn, Henk-Willem Veltkamp, Yiyuan Zhao, Remco Sanders, Yaxiang Zeng and Thomas Schut.
**Proceedings:** Dennis Alveringh.

# MICRO CORIOLIS MASS FLOW SENSOR WITH INTEGRATED RESISTIVE PRESSURE SENSORS

*J. Groenesteijn[1], D. Alveringh[2], T.V.P. Schut[2], R.J. Wiegerink[2], W. Sparreboom[1] and J.C. Lötters[1,2]*
[1] Bronkhorst High-Tech BV, Ruurlo, The Netherlands
[2] MESA+ Institute for Nanotechnology, University of Twente, Enschede, The Netherlands

## ABSTRACT

We report on novel resistive pressure sensors, integrated on-chip at the inlet- and outlet-channels of a micro Coriolis mass flow sensor. The pressure sensors can be used to measure the pressure drop over the Coriolis sensor which can be used to compensate pressure-dependent behaviour that might occur and it can be used to calculate the dynamic viscosity of the fluid inside the channels.

## KEYWORDS

Resistive pressure sensor, micro Coriolis mass flow sensor, multiparameter measurement, viscosity measurement

## INTRODUCTION

We report on novel resistive pressure sensors, integrated on one chip with a micro Coriolis mass flow sensor. The two pressure sensors are placed on the inlet- and outlet-channels of the Coriolis mass flow sensor, which not only allows the measurement of the in- and outlet pressure, but also the pressure drop over the flow sensor. By using the quantities measured by the Coriolis sensor (mass flow and density) together with the pressure drop, the dynamic viscosity can be measured in real-time as is shown schematically in Figure 1. The pressure measurement can also be used to compensate pressure-dependent behaviour of the Coriolis sensor. The pressure sensor consists of a Wheatstone bridge of metal tracks meandering over a channel. As a result, the design of the fluidic path of the Coriolis sensor [1] and the fabrication process [2] do not have to be adjusted to add the pressure sensors to the flow sensor.

In the past, many microfluidic sensors have been made using their own unique fabrication process, e.g. Coriolis flow sensors [3, 4] and pressure sensors [5, 6]. However, since these fabrication processes are unique, combining these sensors on the same chip is hard to achieve. In [7], we integrated a capacitive pressure sensor with a micro Coriolis mass flow sensor. However, this pressure sensor suffered from low sensitivity and large drift. Due to crosstalk between the different capacitive read-outs, these pressure sensors and the Coriolis sensor could not be read out simultaneously. The resistive pressure sensors presented here consist of a Wheatstone bridge which is actuated and read out using a lock-in amplifier. As a result, the sensitivity is higher, the drift lower and it can be operated together with the Coriolis sensor.

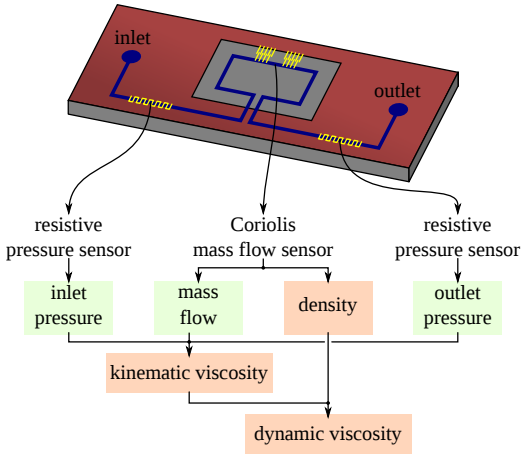


*Figure 1: Overview of the integrated multiparameter measurement system. The output of the pressure sensors and the Coriolis sensor can be used to determine the viscosity of the fluid.*

## THEORY

The design of the pressure sensors is shown schematically in Figure 2 and an SEM image is shown in Figure 3.[8] The resistive pressure sensors consist of a channel with the four resistors of the Wheatstone bridge on top. Each resistor consists of 123 strain gauges placed perpendicular to the direction of the channel and the (unstrained) sections that connect these together. When a pressure is applied inside the channel, the flat top will deform. Two of the resistors are placed in the center of the channel, where the flat top of the channel will elongate the strain gauges due to the deformation of the top and will thus increase in resistance. The two other resistors are placed at the edge of the channel, close to where it is anchored in the silicon bulk. The deformation will cause a compression of the strain gauge and will thus decrease the resistance. The input voltage of the Wheatstone bridge is applied by the

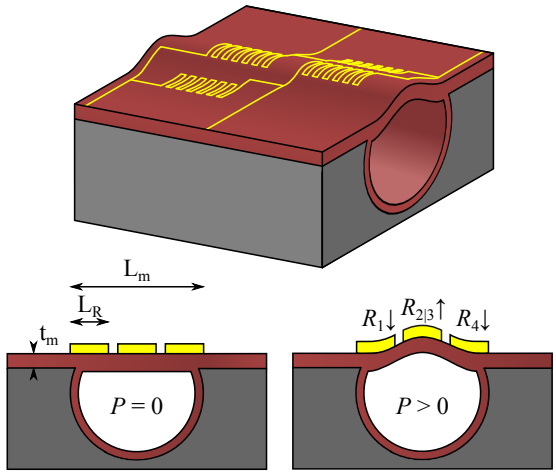


*Figure 2: Illustration of the design of the resistive pressure sensor. The flat part at the top of the channel will deform due to an applied pressure. The thin-film resistors on top will then elongate or compress due to this deformation.*

function generator in a Stanford Research SR830 lock-in amplifier and the output voltage is measured by the same lock-in amplifier. The output voltage is equal to:

$$V_{\text{out}} = V_{\text{in}} \left( \frac{R_2}{R_1 + R_2} - \frac{R_4}{R_3 + R_4} \right) \tag{1}$$

All resistances are designed to be equal when no pressure is applied and the resistances can be rewritten as:

$$\begin{aligned} R_1 = R_4 &= R_0 - \Delta R_{1,4}, \\ R_2 = R_3 &= R_0 + \Delta R_{2,3} \end{aligned} \tag{2}$$

When substituting equation (2) into equation (1) and assuming the change in resistance is much smaller than the initial value the output voltage can be calculated using:

$$V_{\text{out}} = V_{\text{in}} \frac{\Delta R_{2,3} + \Delta R_{1,4}}{2R_0} \tag{3}$$

Here $R_0$ contains both the initial resistance of the strain gauges as the resistance of the parts connecting them. To estimate $\Delta R_{2,3}$ and $\Delta R_{1,4}$, the deformation has been simulated using Comsol Multiphysics. Since the deformation in the length-direction of the channel will be constant, a 2D simulation of the cross-section of the channel will suffice to simulate the deformation of one strain gauge. Separate simulations were performed for the elongating and compressing resistors using a pressure range of 1 to 10 bar. The resulting change in length is shown in Figure 4. The deformation of the two different strain gauges is not equal, indicating that $\Delta R_{2,3} \neq \Delta R_{1,4}$. The deformation is in the order of a few nm on strain gauges of $40\,\mu\text{m}$, indicating a change in resistance less than $0.1\,\%$ of the unstrained value.

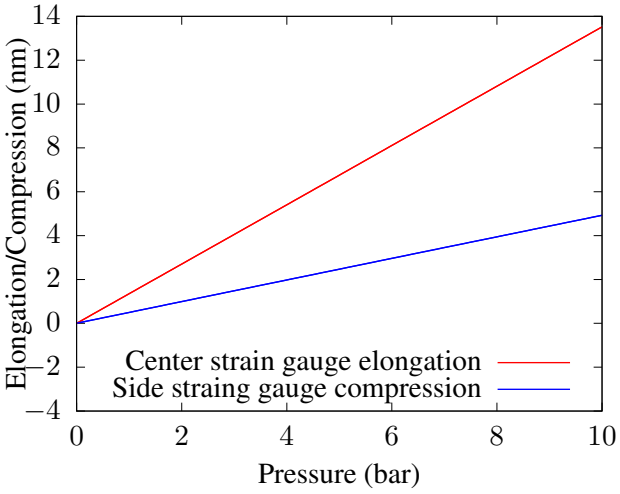


*Figure 4: Simulated change in strain gauge length for the elongating and compressing resistors. The initial length of each is* $40\,\mu\text{m}$.

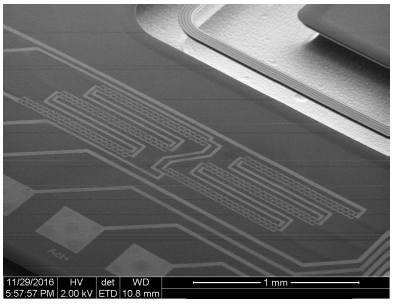


*Figure 3: SEM image of the fabricated resistive pressure sensor. To reduce the pressure drop over the in- and outlet channels, three parallel channels are used. A single pressure sensor is placed on all three, measuring the average pressure inside the three channels.*

## EXPERIMENTAL

To characterize the sensors, gauge pressures have been applied in the range of 0 to $1\,\text{bar}$ in steps of $0.1\,\text{bar}$. The results of these measurements are shown in Figure 5. The amplitude of the applied voltage $V_{\text{in}}$ is $100\,\text{mV}$ at a frequency of $1.5\,\text{kHz}$. The results show a linear response with a sensitivity of $4\,\mu\text{V}\,\text{bar}^{-1}$ without any noticeable hysteresis. Tests show that the burst pressure is higher than $10\,\text{bar}$. The pressure drop is measured together with the mass flow for water and isopropyl alcohol (IPA) in a flow-range of $0\,\text{g}\,\text{h}^{-1}$ to $12\,\text{g}\,\text{h}^{-1}$ with a pressure at the inlet of 3 and $4\,\text{bar}$. The results of these measuremnets are shown in Figure 6. Future work will include design optimization for the pressure sensor and characterization of the different parameters that can be measured using multiple fluids.

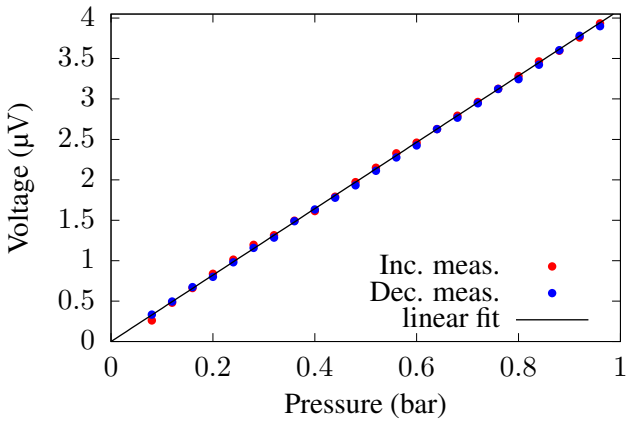


*Figure 5: Characterization of the pressure sensor with a pressure applied by a pressure controller in the range of* 0 bar *to* 1 bar. *There was no fluid flow during the measurement.*

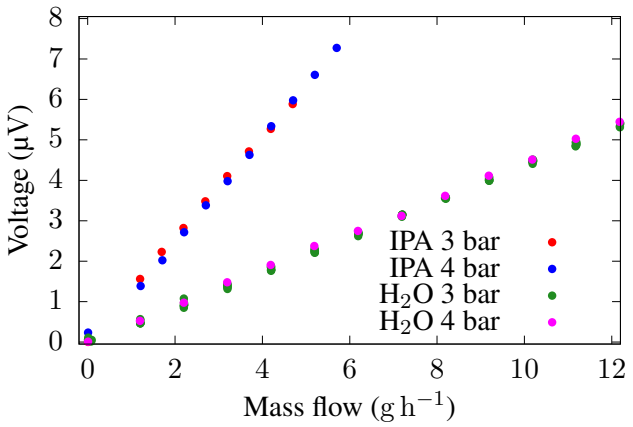


*Figure 6: Measurement of the pressure drop over the sensor at varying flow rates of both water and IPA. The measurements are done using an input pressure of 3 and* 4 bar.

## APPLICATIONS

### Compensation

The fabrication process allows to make free hanging channels with a very thin channel wall. This makes a sensor made using these channels very sensitive to properties of the fluid inside the channel. For the pressure sensor, the deformation of the channel due to pressure results in an accurate pressure measurement. However, in the Coriolis mass flow sensor, this deformation changes the stiffness of the channel and will thus result in a pressure dependent resonance frequency of the sensor. Since flow introduces a pressure drop over the length of the vibrating channel, this too adds a pressure dependence. This can be seen in Figures 7 and 8 where the resonance frequency is measured during a flow measurement using IPA and during static measurements using mixtures of water and IPA. When assuming that

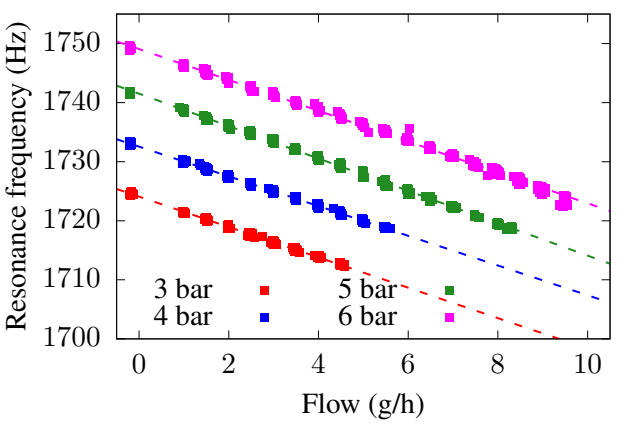


*Figure 7: Measured resonance frequency of the Coriolis mass flow sensor for different flow and input pressure. The used fluid is IPA.*

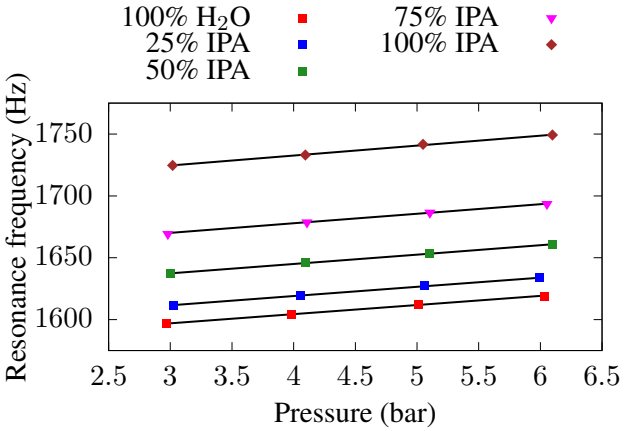


*Figure 8: Measured resonance frequency of the Coriolis mass flow sensor for different mixtures of water and IPA at different input pressures. The black lines indicate the calculated frequency using equation* (4).

the stiffness of the channel is linearly proportional to the pressure, the resonance frequency can be calculated using:

$$\omega_0 = \sqrt{\frac{k_0 + \alpha \cdot P}{m_{channel} + \rho \cdot V_{channel}}}, \qquad (4)$$

where $\omega_0$ is the resonance frequency, $k_0$ is the spring constant of the channel without an applied pressure, $\alpha$ is a calibrated value indicating the pressure dependence of the stiffness, $P$ is the pressure in the channel, $m_{channel}$ is the mass of the channel, $\rho$ the density of the liquid and $V_{channel}$ the volume of the liquid inside the channel. Using the results in Figure 8 for pure water and pure IPA, $\alpha$ and $k_0$ can be calibrated. The resulting modelled resonance frequencies are indicated using black lines.

### Viscosity

The pressure drop over a channel, the mass flow through that channel and the density of the fluid in that

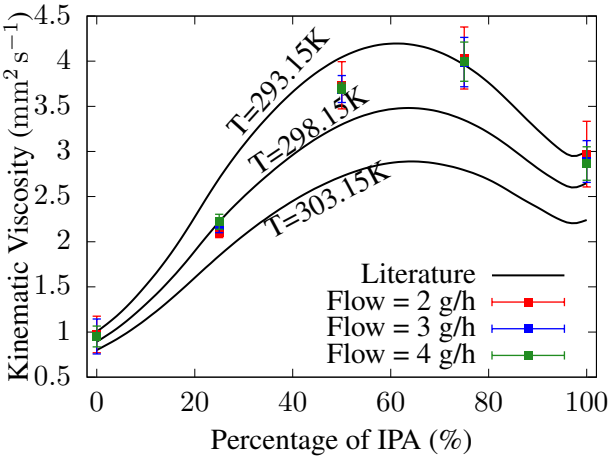


*Figure 9: The kinematic viscosity of mixtures of water and IPA. Measurements from [9] are shown as reference values.*

channel can be used to find the dynamic viscosity of liquids. To do this, the Hagen-Poiseuille equation has to be rewritten to:

$$\mu = \frac{\pi \Delta P \rho D_h^4}{128 L \Phi_m}, \tag{5}$$

where $\mu$ is the dynamic viscosity of the fluid, $\Delta P$ is the pressure drop over the channel, $\rho$ is the density, $D_h$ is the hydraulic diameter of the channel, $L$ is the length of the channel and $\Phi_m$ is the mass flow.

The Coriolis flow sensor can already be used to measure the density and mass flow, so combined with the pressure sensors, the dynamic viscosity can be determined. Figure 9 shows the results for different mixtures of water and IPA. A calibration using pure water was used to calculate the viscosity using the output of the different sensors. Since the temperature of the fluid in the channel could not be measured during the measurements and the viscosity is heavily dependent on the temperature, the calibration is done at 17 and 21 degrees Celsius. The figure also shows the measured viscosity of the mixtures according to [9].

## CONCLUSION

We report on resistive pressure sensors, integrated with a micro Coriolis mass flow sensor. The pressure sensor has a linear response with a sensitivity of $4\,\mu\mathrm{V\,bar^{-1}}$ in the range of 0 to 1 barg. The integrated pressure sensors have been used to compensate the pressure-dependence of the stiffness of the free-hanging channel in the micro Coriolis mass flow sensor, improving its accuracy. By using the measurements of the pressure sensors and the micro Coriolis mass flow sensor, the viscosities of several mixtures of water and IPA have been determined.

## REFERENCES

[1] W. Sparreboom, et al., “Compact mass flow meter based on a micro Coriolis flow sensor”, Micromachines, 4(1), pp.22-33, 2013

[2] J. Groenesteijn et al., “A versatile technology platform for microfluidic handling systems, partÂăI: fabrication and functionalization”, Microfluidics and Nanofluidics, 21 (7), pp. 127, 2017

[3] P. Enoksson et al., “A silicon resonant sensor structure for Coriolis mass-flow measurements”, Journal of Microelectromechanical Systems, vol. 6, no. 2, pp. 119-125, Jun 1997

[4] J. Haneveld et al., “Modeling, design, fabrication and characterization of a micro Coriolis mass flow sensor”, Journal of Micromechanics and Microengineering, vol. 20, 2010

[5] W. P. Eaton et al., “Micromachined pressure sensors: review and recent developments”, Smart Materials and Structures, vol. 6, no. 5, p. 530, 1997

[6] Y. Zhang et al., “A high-sensitive ultra-thin MEMS capacitive pressure sensor”, in The 16th International Solid-State Sensors, Actuators and Microsystems Conference (TRANSDUCERS). IEEE, 2011, pp. 112-115

[7] J. C. Lötters et al., “Integrated multi-parameter flow measurement system”, in The IEEE 27th International Conference on Micro Electro Mechanical Systems (MEMS). IEEE, 2014, pp. 975-978

[8] D. Alveringh et al., “Resistive pressure sensors integrated with a Coriolis mass flow sensor”, accepted at The 19th International Solid-State Sensors, Actuators and Microsystems Conference (TRANSDUCERS). IEEE, 2017

[9] F.-M. Pang et al., “Densities and viscosities of aqueous solutions of 1-propanol and 2-propanol at temperatures from 293.15K to 333.15K”, Journal of Molecular Liquids, vol. 136, no. 1, pp. 71-78, 2007.

## CONTACT

* J. Groenesteijn, j.groenesteijn@bronkhorst.com